International Journal of Hydrogen Energy 78 (2024) 1004–1015

Contents lists available at ScienceDirect

International Journal of Hydrogen Energy

journal homepage: www.elsevier.com/locate/he

The mechanism of propagation of NH_3/air and NH_3/H_2/air laminar premixed flame fronts

Efstathios-Al. Tingas [a], Savvas Gkantonas [b], Epaminondas Mastorakos [b], Dimitris Goussis [c,d,*]

[a] School of Computing, Engineering and the Built Environment, Edinburgh Napier University, Edinburgh, EH10 5DT, UK
[b] University of Cambridge, Department of Engineering, Cambridge, UK
[c] Khalifa University, Department of Mechanical and Nuclear Engineering, Abu Dhabi, United Arab Emirates
[d] Research and Innovation Center on CO_2, and H_2, Khalifa University, Abu Dhabi, United Arab Emirates

ARTICLE INFO

Keywords:
Premixed flames
Asymptotics
Ammonia
Hydrogen
CSP
Flame structure

ABSTRACT

The mechanism of flame front propagation in NH_3/air and NH_3/H_2/air steady, laminar premixed flames is examined. Since the process is characterised by a state of chemical non-equilibrium, the analysis focuses on the explosive mode that is introduced by chemical kinetics. The chemistry expressed in this mode is the one that tends to lead the system away from equilibrium and sustains the chemical non-equilibrium state. The algorithmic tools of Computational Singular Perturbation method are employed, so the analysis is not hindered by the size of the detailed chemical kinetics mechanism employed. Under engine-relevant conditions and a stoichiometric mixture, it is shown that in the NH_3/air case the flame front propagation is driven by reaction $NH_2 + NO \rightarrow NNH + OH$ far from the front and by reaction $H + O_2 \rightarrow OH + O$ closer to the front; the latter assisted by reaction $H_2 + OH \rightarrow H_2O + H$. These reactions are mainly responsible for the heat released, by effectively feeding the most exothermic reactions, which are OH-consuming. The ensuing chemical activity in the neighbourhood of maximum heat release rate generates upstream diffusion of heat, NH_2, NO, H and H_2, which initiate the chemical activity ahead of the flame front. This mechanism of front propagation is promoted by H_2 addition in the mixture, by reinforcing the action of these three reactions and by activating another OH-producing reaction $O+H_2 \rightarrow OH+H$. A preliminary investigation of lean mixtures indicated that this flame front propagation mechanism is also present in the case of a pure ammonia fuel. However, when H_2 is present in the initial mixture, significant changes are observed that relate to the prevailing lower temperatures and the decreased upstream diffusion of heat. These findings provide novel insights with direct implications for controlling and optimising NH_3 and NH_3/H_2 flames planned for engine applications. The approach proposed here can also be extended for analysing flame propagation mechanisms across a more diverse spectrum of fuel mixtures and flame configurations, offering invaluable support to technologies pivotal in the ongoing energy transition efforts.

1. Introduction

Ammonia combustion's wide-ranging research [1,2] and ongoing development of practical ammonia-fuelled devices [3,4] underscore its recognition as a promising renewable, zero-carbon fuel option. Consequently, many studies on the combustion characteristics of ammonia (NH_3) have become recently available with the aim to investigate challenges, such as low flammability, high ignition delay and nitrogenous emissions, as well as improvements to the above with the addition of hydrogen or hydrocarbon fuels in the initial mixture [5].

Regarding hydrogen addition, Lee et al. [6] studied both experimentally and computationally the effect of its addition on the flame speed, stretch and structure in the context of ammonia/air premixed flames. Their work revealed that hydrogen addition can enhance the flame speed, the flame sensitivity to stretch and amend the flame structure by enhancing nitrogen oxides (NOx) and nitrous oxide (N_2O) formation. Ichikawa et al. [7] employed spherically propagating laminar flames to study experimentally the effect of hydrogen addition on the laminar burning velocity and Markstein length of ammonia/hydrogen/air premixed flames from 1 to 5 atm. Cheng et al. [8] used one-dimensional simulations to investigate the flame structure of premixed laminar NH_3/air flames at different equivalence ratios both at atmospheric and high pressures, and proposed the use of three heat release rate markers based on selected concentrations of chemical species, namely, the $[NH_3][OH]$, $[NH_2][O]$ and $[NH_2][H]$. Tang et al. [9]

* Corresponding author.
E-mail address: dimitris.goussis@ku.ac.ae (D. Goussis).

https://doi.org/10.1016/j.ijhydene.2024.06.289
Received 15 April 2024; Received in revised form 18 June 2024; Accepted 21 June 2024
Available online 2 July 2024

undertook an experimental campaign in order to investigate the effects of the equivalence ratio, mixing gas ratio, flow rate and inlet temperature of mixture on the combustion limit characteristics of ammonia-hydrogen and ammonia-methane flames. Osipova et al. [10] performed an experimental and numerical study on ammonia/hydrogen premixed flames at atmospheric conditions and in a wide range of equivalence ratios (0.7–1.5) and compared measured species profiles against those obtained from four different detailed chemical kinetics mechanisms. Yang et al. [11] performed direct numerical simulations (DNS) of turbulent premixed ammonia-hydrogen flames under engine-relevant conditions (445 K and 0.54 MPa), and reported that high/low heat release rate values occurred in the concave/convex flame areas and that the turbulent burning velocity was favoured at fuel lean than fuel rich conditions. More recently, Hu et al. [12] reported through the use of experiments that the increase of the hydrogen content enhances the hydrodynamic instability and leads to the decrease of the flame thickness and critical instability radius. Thomas et al. [13] used a concentric tube burner to study axi-symmetric diffusion flames of ammonia/hydrogen blends and assessed the accuracy of existing chemical kinetics models in a wide range of hydrogen share. Zhang et al. [14] used a swirl combustor to investigate experimentally the blowoff limits and emissions of ammonia/hydrogen blends under various global equivalence ratio, hydrogen blending ratio, inlet gas temperature, combustor wall conditions and swirl numbers and reported that the optimal emission control occurred at stoichiometric conditions and robust flames were obtained at hydrogen blending ratio over 20%.

Some considerable work has also been reported on the kinetics of ammonia/hydrogen combustion. Rocha et al. [15] assessed the performance of ten chemical kinetics mechanisms against experimental results of ignition delay times, laminar flame speeds and NOx concentrations for premixed mixtures of NH_3/air and NH_3/H_2/air. The authors reported poor accuracy of the examined kinetics mechanisms and a relatively poor consistency on the most important reactions identified through the sensitivity analysis; i.e., in some mechanisms the second most reaction was H + NO (+M) ↔ HNO (+M), while in other mechanisms this reaction was not present at all. Nevertheless, the study consistently indicated reaction $H + O_2 \leftrightarrow O + OH$ having the largest influence on the flame speed. Mashruk et al. [16] examined an axial swirl burner fuelled with a NH_3/H_2/air mixture that was simulated by a network of four perfectly stirred reactors (PSR) to model the pre-mixing, flame, central recirculation zone (CRZ) and external recirculation zone (ERZ) at three different equivalence ratios (0.8, 1.0, 1.2). The authors performed a rate of production analysis focusing on NH_3, NO, NO_2 and N_2O with the purpose of identifying the key reactions for the production/depletion of these species. The two most important reactions for the depletion of NH_3 were reported to be $NH_3 + OH \leftrightarrow H_2O + NH_2$ and $NH_3 + H \leftrightarrow H_2 + NH_2$. Liang et al. [17] performed an experimental study on the dynamics of a premixed NH_3/H_2/air flame in a duct of different ammonia mixing ratios, accompanied by simulations of freely propagating premixed laminar flames simulations and relevant sensitivity analysis with different chemical kinetics mechanisms. The authors underlined the importance of H, OH and NH_2 radicals as well as the chain branching reaction $H + O_2 \leftrightarrow O + OH$ (promoting a faster flame speed), and $NH_2 + NO \leftrightarrow N_2 + H_2O$, $NH_2 + NH \leftrightarrow N_2H_3$ (promoting a slower flame speed). Wu et al. [18] investigated numerically the effects of initial temperature/pressure, hydrogen ratio and equivalence ratio on the flame speed of premixed NH_3/H_2/air flames in the context of 1d laminar flames at engine relevant conditions. Using sensitivity analysis, they showed that the chain branching reaction $H + O_2 \leftrightarrow O + OH$ has the largest (positive) influence on the flame speed at all examined conditions. Reaction $H + O_2$ (+M) ↔ HO_2 (+M) was identified as the second most important reaction, with an inhibiting effect on the flame speed. Third and fourth in the row were reactions $NH_3 + O_2 \leftrightarrow HO_2 + NH_2$, $NH_3 \leftrightarrow H + NH_2$, both with inhibiting effect on the flame speed. Alnasif et al. [19] performed an experimental and numerical review of the literature on laminar flame speeds of premixed ammonia/hydrogen blends at 70/30 (%vol) ratio. In this work, the performance of 36 published chemical kinetics mechanisms was assessed against the available experimental data. The authors reported that the best performing mechanisms demonstrated different reaction routes in view of sensitivity analysis. Such analysis highlighted the importance of $H + O_2 \leftrightarrow O + OH$, $NH_2 + NH_2 \leftrightarrow N_2H_2 + H_2$, $OH + H_2 \leftrightarrow H + H_2O$, $H + O_2(^+M) \leftrightarrow HO_2(^+M)$, $NH_2 + H \leftrightarrow NH + H_2$, and $NH_2 + O \leftrightarrow HNO + H$; the former three promoting and the latter three retarding the flame speed. Another recent chemical kinetics study by Zhu et al. [20] proposed a new detailed kinetics mechanism for the combustion chemistry of NH_3 and NH_3/H_2 mixtures. The mechanism was extensively validated against a wide range of experimental data reported in the literature, namely ignition delay times, laminar flame speeds and species profiles. With regard to the flame speed, the sensitivity analysis pointed to the importance of $H + O_2 \leftrightarrow O + OH$, $NH_2 + NH \leftrightarrow N_2H_2 + H$, $NH_2 + NO \leftrightarrow NNH + OH$, $H_2 + O \leftrightarrow H + OH$, all of them promoting the flame speed.

All these studies have been instrumental in advancing our understanding of NH_3 and NH_3/H_2 combustion; in part by validating a large number of chemical kinetics mechanisms against experimentally observed laminar burning velocity (LBV); e.g., [5,21]. Yet, as it is evident from the above discussion, the structure and propagation mechanism of NH_3 flames are not yet as well understood as for hydrocarbon or H_2 flames. For the latter, our fundamental understanding is primarily based on asymptotic analyses that extended the pioneering work of Lewis and von Elbe and of Zeldovich and Frank-Kamenetski [22,23]. These analyses provided detailed insights on flame front propagation mechanisms, by allowing a quantification of the important phenomena present across flames [24,25] and by extension, the exploration of flame-flow interactions that might occur [26,27].

Employing asymptotic analytic methods, especially the more realistic “rate-ratio” type [24–26], could serve as a promising pathway to better understanding NH_3 flame propagation, enabling enhanced flame control and optimisation for practical devices. However, their use is hindered by the requirements for (i) constructing a reduced mechanism, (ii) identifying the length of various layers across the flame (e.g., preheat, fuel consumption, H_2-oxidation layers) and (iii) introducing matching conditions to connect these layers. The choices on these issues are, almost exclusively, based on the investigator’s experience and elaborate paper-and-pencil analysis. As a result, the increasing size of the available chemical kinetics mechanisms has progressively necessitated more complex calculations and resulted in fewer asymptotic studies, hence proving the difficulty in applying the same techniques to NH_3 and other new emerging fuels. Here, the applicability of asymptotic analysis will be extended for the case of detailed chemical kinetics mechanisms for NH_3/air and NH_3/H_2/air combustion by employing Computational Singular Perturbation (CSP) [28,29], which is most suited for the study of complex multi-scale reacting systems and can generate, order by order, the results of asymptotic analysis [30,31]. CSP has been extensively used to construct reduced mechanisms and to analyse many reacting configurations [32–34]. CSP identifies (i) the low dimensional surface in phase space (a.k.a., slow invariant manifold or SIM) on which the reacting process is confined to evolve and (ii) the slow model that governs the evolution along the SIM. In the presence of both transport and chemistry, CSP can algorithmically (a) determine whether transport or chemistry drives the evolution along the SIM and (b) identify the dominant reactions involved.

The main objective of this paper is to identify the propagation mechanism of NH_3/air and NH_3/H_2/air steady, laminar, premixed flame fronts at engine-relevant conditions. In this canonical configuration, it is known that a state of chemical non-equilibrium is established with some chemical dynamics modes tending to lead the system towards chemical equilibrium (dissipative modes), while others tend to lead it away from it (explosive modes) [28,34,35]. Here, all chemical kinetics modes will be accounted for, and the chemical activity reported in each mode will be assessed. However, the emphasis will be placed on the

fastest explosive mode, which is the one that can sustain the chemical activity required for the flame to propagate. Moreover, the role of the explosive mode in influencing flame propagation will be assessed, and the regions of the flame where such an influence is manifested will be determined.

2. Problem definition and CSP tools

Isobaric, laminar, premixed flame propagation is governed by a system of the form:

$$\frac{d\mathbf{z}}{dt} = \sum_{n=1}^{N+1} \widehat{\mathbf{S}}_{c,n} + \sum_{n=1}^{N+1} \widehat{\mathbf{S}}_{d,n} + \sum_{k=1}^{2K} \widehat{\mathbf{S}}_k R^k = \mathbf{g}(\mathbf{z}) \tag{1}$$

where $\mathbf{z} = [\mathbf{y}, T]^T$ is the $(N+1)$-dim. column state vector of the N species mass fractions and temperature, $\widehat{\mathbf{S}}_{c,n}$ and $\widehat{\mathbf{S}}_{d,n}$ represent the convection and diffusion operators of the nth component of $\mathbf{z}$ ($n = 1, N+1$), and $\widehat{\mathbf{S}}_k$ and R^k are the generalised stoichiometric vector and reaction rate of the kth reaction ($k = 1, 2K$), respectively. The forward and backward directions of each of the K reactions are considered separately in order to assess the role of each [32,36]; see Supplemental Material for details. In CSP form, Eq. (1) is cast in the form:

$$\frac{d\mathbf{z}}{dt} = \sum_{n=1}^{N+1} \mathbf{a}_n h^n \tag{2}$$

$$h^n = \mathbf{b}^n \cdot \mathbf{g}(\mathbf{z}) = \sum_{l=1}^{N+1} \gamma_l^n + \sum_{l=1}^{N+1} \delta_l^n + \sum_{k=1}^{2K} \varepsilon_k^n \tag{3}$$

where $\mathbf{a}_n$ is the nth CSP basis column vector, $\mathbf{b}^n$ is the related dual row vector ($\mathbf{b}^i \cdot \mathbf{a}^j = \delta_j^i$) and h^n is the nth modal amplitude [28,29]. For consistency, the amplitude h^n is set positive, by properly changing the sign of $\mathbf{b}^n$ and $\mathbf{a}_n$ [36]. The terms $\gamma_l^n = \mathbf{b}^n \cdot \widehat{\mathbf{S}}_{d,l}$ and $\delta_l^n = \mathbf{b}^n \cdot \widehat{\mathbf{S}}_{c,l}$ denote the contribution of the lth convection and diffusion operators in $\widehat{\mathbf{S}}_{c,l}$ and $\widehat{\mathbf{S}}_{d,l}$ to the amplitude h^n, while the term $\varepsilon_k^n = \mathbf{b}^n \cdot \widehat{\mathbf{S}}_k R^k$ denotes the contribution of the kth reaction $\widehat{\mathbf{S}}_k R^k$. The CSP vectors $\mathbf{a}_n$ denote directions in phase space, along which the recorded chemical activity is characterised by the time scale τ_n. This time scale is approximated by the relation $\tau_n = |\lambda_n|^{-1}$, where λ_n is the nth eigenvalue of the Jacobian $\mathbf{J}$ of the chemical kinetics term in Eq. (1); $\tau_1 < \tau_2 < \cdots$. When the real part of λ_n is positive (negative) the related time scale is explosive (dissipative) [28,37]. The CSP basis vectors $\mathbf{a}_n$ and $\mathbf{b}^n$ can be approximated to leading order by the right and left eigenvectors of $\mathbf{J}$ [28,30].

The time scale characterising the activity along each $\mathbf{a}_n$ might not always coincide with τ_n that characterises chemical activity, since transport might dominate along this direction. In particular, since the fastest time scales are introduced by chemistry [33,38], the fastest time scales, say $\tau_1 < \cdots < \tau_M$, will characterise the action along the fastest directions $\mathbf{a}_1$ to $\mathbf{a}_M$. However, the characteristic time scales along the slower directions might originate from transport [39,40]. The requirement for the chemistry-based time scale τ_n to characterise the action along a certain slow $\mathbf{a}_n$ is that the contribution of chemistry to the related h^n is significant [29,41].

For the steady process considered here, all amplitudes in Eq. (2) vanish; i.e., $h^n = 0$ for $n = 1, N+1$. This feature denotes that convective, diffusive and chemical activity are in equilibrium. The directions $\mathbf{a}_n$, along which there is significant chemical activity recorded, denote a chemical non-equilibrium state. Of particular interest is the direction that is characterised by the fastest explosive time scale, say τ_e [28, 42]. This is because the chemical reactions acting along this direction, say $\mathbf{a}_e$, are those that tend to lead the system away from equilibrium and can thus support the propagation of a flame front. The explosive time scale τ_e is among the slow ones, so it is not guaranteed that it can characterise the evolution of the reacting process, since transport might have a dominant presence along $\mathbf{a}_e$. Therefore, the degree to which chemistry contributes to its amplitude h^e is a decisive factor on whether the explosive mode can provide meaningful diagnostics.

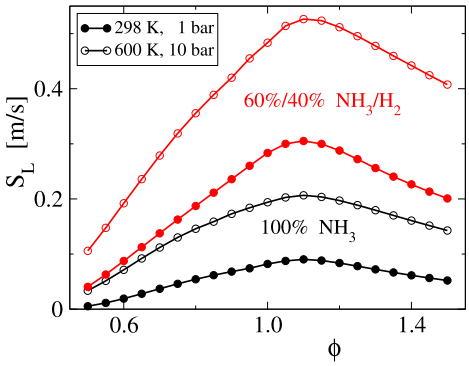

Fig. 1. The ϕ-dependence of S_L for 100% NH_3 and 60%/40% (v/v) NH_3/H_2.

The analysis of the explosive mode will be carried-out with CSP algorithmic tools; the *Time scale Participation Index* (TPI), the *Amplitude Participation Index* (API) and the *Pointer* (Po). The *TPIs* of the nth mode J_k^n measure the contribution of the kth reaction to τ_n [36,37]. Positive (negative) values of J_k^n promote the explosive (dissipative) character of the mode. The indices are normalised so that $|J_1^n| + \cdots |J_{2K}^n| = 1$. The *APIs* of the nth mode, $P_{co,l}^n$, $P_{di,l}^n$ and $P_{ch,k}^n$ measure the contribution of each of the $N+1$ convection and diffusion operators and of the $2K$ reactions to h^n; positive (negative) values of these indices tend to promote (oppose) the impact of the mode [32,33]. These indices are normalised so that $P_{con}^n + P_{dif}^n + P_{che}^n = 1$, where $P_{con}^n = |P_{co,1}^n| + \cdots + |P_{co,N+1}^n|$, $P_{dif}^n = |P_{di,1}^n| + \cdots + |P_{di,N+1}^n|$ and $P_{che}^n = |P_{ch,1}^n| + \cdots + |P_{ch,2K}^n|$. Finally, the *Po* identifies the variables associated the most to the nth mode [28,32,37]. See Supplemental Material for details on the CSP tools.

Here, the detailed chemical kinetics mechanism developed by Han et al. [21] is employed. The mechanism consists of $N = 36$ species and $K = 298$ reactions and has been successfully validated in shock-tube and premixed-flame experiments. The solutions of the governing equations reported here were obtained with Cantera and the CSP diagnostics were obtained with our in-house Fortran code.

3. Results and discussion

3.1. Laminar burning velocity

The influence of H_2 on the LBV is examined by considering that the fuel is either 100% NH_3 or a mixture of 60% NH_3 and 40% H_2 by volume, which are hereafter referred to as 0%- and 40%-H_2 cases. Fig. 1 displays the LBV, S_L, as a function of equivalence ratio, ϕ, for two sets of initial pressure and temperature. A case of 1 bar and 298 K is first considered as a reference, in addition to an engine-like condition of 10 bar and 600 K that is also within the validity range of the chemical mechanism employed. Consistent with many studies (e.g., see [5,43]), Fig. 1 shows that LBV increases with the presence of H_2 in the mixture and this becomes more pronounced as the percentage of H_2 increases; see also Fig. S1. The issue that will be explored next is the mechanism via which the presence of H_2 in the initial mixture influences the LBV; i.e., whether it simply promotes the mechanism that exists when absent or whether it introduces a new mechanism. The analysis hereafter will focus on a stoichiometric mixture and the engine-like conditions.

3.2. Flame structure

Fig. 2 displays the profiles of the time scales τ_n and the temperature T (top) and the profiles of P_{dif}^e, P_{con}^e and P_{che}^e (bottom) in the 0%-H_2 and 40%-H_2 cases. It is shown that the spatial scale in the 40%-H_2 case is shorter, since the flame thickness is shorter. This feature is

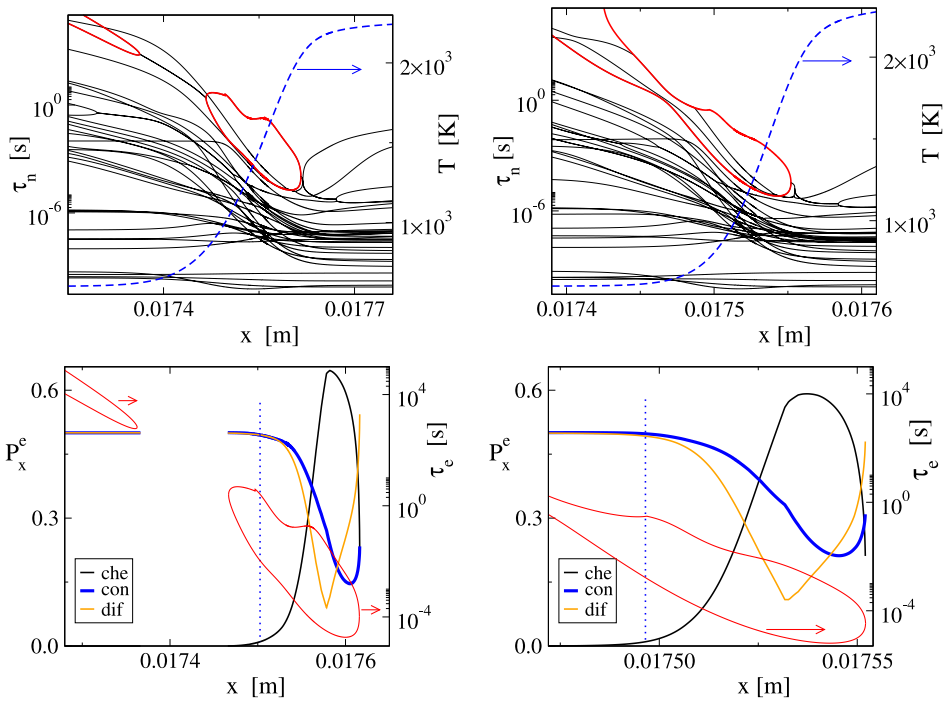

Fig. 2. Spatial profiles of time scales τ_n of all modes (explosive in red and dissipative in black) and of temperature (top) and of P^e_{dif}, P^e_{con}, P^e_{che} and the explosive time scale τ_e (bottom); the latter superimposed on the profiles of the explosive time scale τ_e. Left 0%-H_2 case and right 40%-H_2 case; T_o = 600 K, p_o = 10 bar, $\phi = 1$. The vertical dotted line denotes the point where $P^e_{che} = 0.01$. (For interpretation of the references to colour in this figure legend, the reader is referred to the web version of this article.)

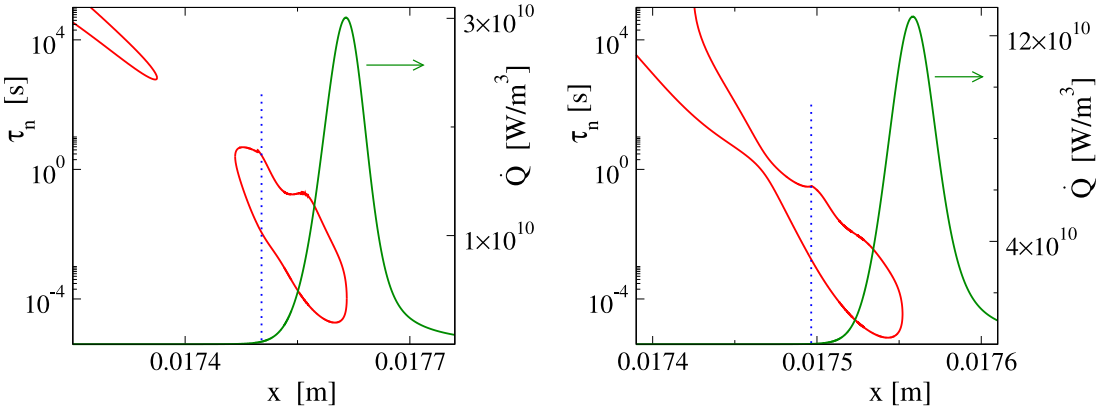

Fig. 3. Spatial profiles of the heat release rate (HRR) $\dot{Q}$ for the 0%-H_2 case (left) and 40%-H_2 case (right), superimposed on the profiles of the explosive time scale τ_e; T_o = 600 K, p_o = 10 bar, $\phi = 1$. The vertical dotted line denotes the point where $P^e_{che} = 0.01$.

exemplified by the different flame velocities; 0.189 m/s in the 0%-case and 0.483 m/s in the 40%-case. It is shown in Fig. 2 that in the 0%-H_2 case there exist two distinct regions in which explosive modes develop; one in the cold region and one during the steep temperature rise. In contrast, in the 40%-H_2 case there is a single explosive region that extends from the cold region to the one where temperature exhibits a steep rise. In both cases, the explosive time scales are among the slowest. The profiles of P^e_{dif}, P^e_{con} and P^e_{che} of the fastest explosive mode, shown in Fig. 2, indicate that its vanishing amplitude $h^e = 0$ sufficiently far from the flame front expresses a balance between the convection and diffusion terms, since $P^e_{dif} = P^e_{con} \approx 0.5$; the contribution of chemistry being negligible ($P^e_{che} \approx 0$). However, as soon as the temperature rises, chemistry starts making significant contributions to the cancellations within the expression $h^e = 0$. Apparently, τ_e, which is based on the chemical kinetics, does not characterise the process far from the flame front, since the activity recorded there within the explosive mode is dominated by transport. Therefore, the analysis of the explosive mode will focus on the region close to the flame front; i.e., downstream the $P^e_{che} = 0.01$ mark, where significant chemical activity is recorded, as shown in Fig. 2. This indicative value of P^e_{che} was selected in order to designate the spatial domain where non-negligible chemical activity starts to be recorded. The significance of the $P^e_{che} = 0.01$ mark is demonstrated in Fig. 3, where it is shown that the steep rise of the heat release rate (HRR) $\dot{Q}$ initiates at this point.

3.2.1. Reactions promoting or opposing the explosive character of the mode

The profiles of the largest *TPI* values for the fastest explosive mode, J^e_k, shown in Fig. 4, indicate that, in the region where chemistry has an active role, the fastest explosive time scale τ_e in both 0% and 40%-H_2 cases is mainly generated by reaction 12f: $O_2 + H \rightarrow OH + O$, followed by 154f: $NH_2 + NO \rightarrow NNH + OH$, 13f: $H_2 + OH \rightarrow H_2O + H$ and 11f: $H_2 + O \rightarrow H + OH$ ($J^e_k > 0$); the latter only in the 40%-H_2 case. The reactions opposing the explosive character of the mode in both cases are mainly 163f: $NH_3 + H \rightarrow NH_2 + H_2$, 161f: $NH_2 + H$ (+ M) $\rightarrow NH_3$ (+ M), 153f: $NH_2 + NO \rightarrow N_2 + H_2O$, 9f: $H + O_2$ (+ M) $\rightarrow HO_2$ (+ M) and 232f: $NH_2 + HNO \rightarrow NH_3 + NO$ ($J^e_k < 0$). An

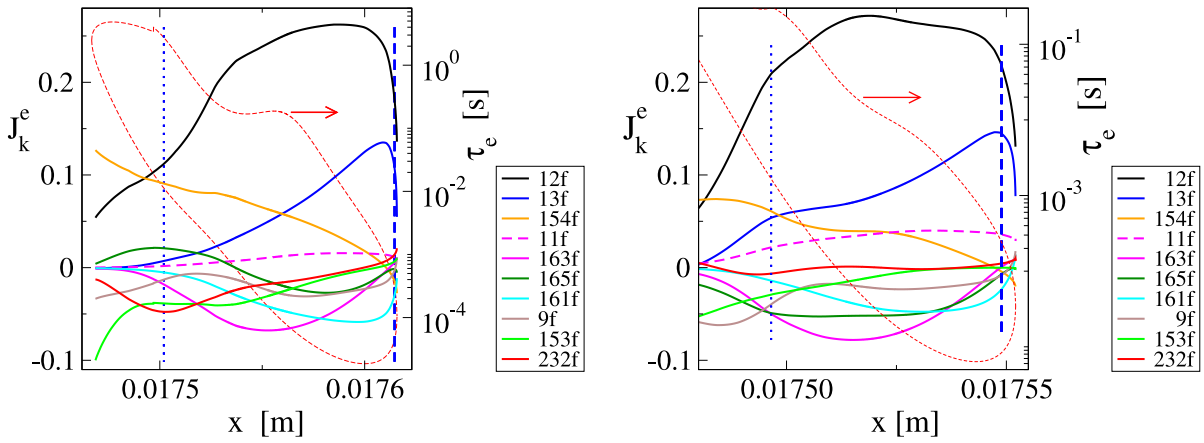

Fig. 4. Spatial profiles of the TPIs J^e_k (k = 1,2K) of the fastest explosive mode for the 0%-H_2 case (left) and 40%-H_2 case (right), superimposed on the profiles of the explosive time scale τ_e; T_o = 600 K, p_o = 10 bar, $\phi = 1$. The vertical dotted line denotes the point where $P^e_{che} = 0.01$ and the vertical dashed line denotes the point of MHRR.

interesting influence in the region of significant chemical activity is exhibited by reaction 165f: $NH_3 + OH \rightarrow NH_2 + H_2O$ that exhibits the largest reaction rate up to the point of maximum HRR (MHRR); in the 0%-H_2 case initially promotes the explosive character of the mode and then opposes it, while in the 40%-H_2 case continuously opposes this character. The promoting reactions 12f, 154f and 11f produce OH, while reactions 13f and 11f produce H that is a reactant of the dominant 12f. The opposing reactions consume NH_2 and H that are reactants of the OH-producing most promoting reactions 12f and 154f. These findings indicate that the chemical activity within the explosive mode focuses on OH-production. Far from the flame front this production is initiated by the nitrogen-chemistry reaction 154f, but is progressively dominated by the hydrogen-chemistry reaction 12f throughout the $P^e_{che} > 0.01$ part, as shown in Fig. 4. A comparison of the J^e_k profiles in Fig. 4 indicate that the major difference in the 0% and 40%-H_2 cases is exhibited by the influence of the promoting reaction 12f, which is stronger in the latter case.

The significance of the OH-producing reactions in establishing the explosive character of the mode is corroborated by the fact that the reactions exhibiting the largest heat release rate (HRR) in the region downstream the $P^e_{che} = 0.01$ mark are the OH-consuming 13f: $H_2+OH \rightarrow H_2O + H$ and 165f: $NH_3 + OH \rightarrow NH_2 + H_2O$ in both 0% and 40%-H_2 cases; see Table S1. The relation of the explosive mode to the heat-released is also manifested by the largest *Po* value (max D^e_i), which points to the temperature throughout the part of the explosive region beyond the $P^e_{che} = 0.01$ mark.

3.2.2. *Reactions and transport processes promoting or opposing the impact of the explosive mode*

The interaction of the chemistry recorded within the fastest explosive mode with transport is highlighted by the largest *API* indices, P^e_x ($P^e_{co,l}$ for convection, $P^e_{di,l}$ for diffusion or $P^e_{ch,k}$ for reactions). Profiles of the largest indices are displayed in Fig. 5; the first and second rows display the indices related to the diffusion and convection operators and the third and fourth rows display those for the forward and backward reactions, respectively.

It was shown in Fig. 4 that in both cases considered the explosive mode expresses an equilibrium between convection and diffusion up to the $P^e_{che} = 0.01$ mark. The top row of Fig. 5 shows that major participants in this equilibrium are heat, ammonia, oxygen and water. Specifically, it is shown that up to the $P^e_{che} = 0.01$ mark, diffusion of heat, NH_3 and O_2 ($D(T)$, $D(NH_3)$, $D(O_2)$) and convection of water ($C(H_2O)$) tend to promote the impact of the explosive mode ($P^e_x > 0$), while convection of heat, ammonia and oxygen ($C(T)$, $C(NH_3)$, $C(O_2)$) and diffusion of water ($D(H_2O)$) tend to oppose it ($P^e_x < 0$). These findings are in agreement with the profiles of temperature and species mass fractions around the $P^e_{che} = 0.01$ mark, displayed in Fig. 6. In particular, the temperature and the mass fraction of water profiles indicate that heat and water diffuse upstream; the former process promoting the chemical activity there ($P^e_x > 0$), while the latter opposing it ($P^e_x < 0$) since water acts as an energy buffer; i.e., non-reacting species that simply absorb heat, thus limiting the increase of the chemical activity [44]. The convection processes have the opposite effect; i.e., the downstream removal of heat opposes the initiation of chemistry, while the removal of the energy buffer promotes it. The mass fraction profiles of NH_3 and O_2 indicate that diffusion tends to accumulate these species in the downstream direction. The diffusion flux of these two species increases with distance as the flame front is approached ($P^e_x > 0$, thus promoting the chemical action in the hot downstream region, where the prevailing conditions facilitate the oxidation process), while the convective flux decreases ($P^e_x < 0$, thus exhibiting an opposing influence).

The upstream equilibrium between convection and diffusion starts breaking up as the flow marches closer to the flame front, due to the action of additional transport processes and of chemical reactions. Specifically, as the second row of Fig. 5 shows, after the $P^e_{che} = 0.01$ mark, the diffusion of NH_2, H_2, NO and later-on of H and OH, start exhibiting a noticeable contribution to the amplitude of the explosive mode, promoting its impact ($P^e_{di,x} > 0$). Towards the end of the explosive period, the influence of the diffusion of NH_2 and H_2 is reversed, while that of NO, H and OH is maintained. Noteworthy in this region are reversals of the influence of additional major transport processes, shown in the top row of Fig. 5; e.g., the diffusion of heat $D(T)$ and ammonia $D(NH_3)$ promotes the impact of the explosive mode ahead of the flame front but opposes near the front. The reversal of the influence of various transport processes within the explosive mode in the region beyond the $P^e_{che} = 0.01$ mark (beyond which a significant chemical activity is recorded), is related to the chemical activity recorded there and can be explained as follows.

(i) Although diffusion of heat $D(T)$ promotes the impact of the explosive mode far from the flame front ($P^e_{di,T} > 0$), it opposes its impact when sufficiently close ($P^e_{di,T} < 0$). This reversal is due to the upstream direction of diffusion, which leads to the removal of heat from the hot rear part and its accumulation at the cold front.

(ii) The diffusion of water $D(H_2O)$ opposes the impact far from the front ($P^e_{di,H_2O} < 0$) and promotes it when close ($P^e_{di,H_2O} > 0$). This is due to the upstream direction of diffusion, which accumulates heat-buffer at the front and removes it from the rear.

(iii) While promoting the impact of the mode far from the flame front ($P^e_{di,NH_3} > 0$), diffusion of ammonia $D(NH_3)$ opposes it when close to it ($P^e_{di,NH_3} < 0$). This is due to the decreasing diffusion

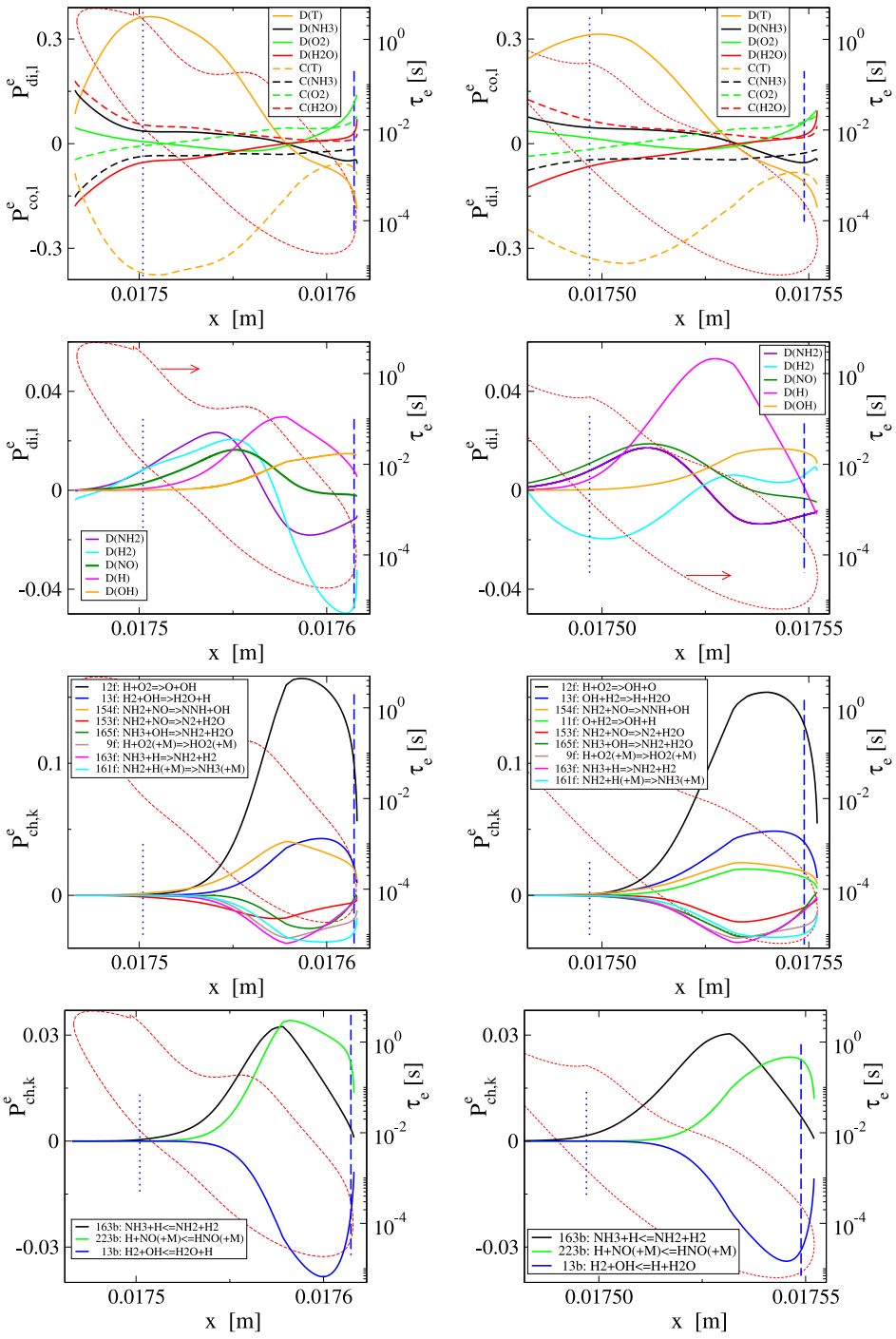

Fig. 5. Profiles of major *APIs* P_x^e of the explosive mode for the 0%-H_2 case (left) and 40%-H_2 case (right); T_o = 600 K, p_o = 10 bar, $\phi = 1$. The vertical dotted and dashed lines as in Fig. 4.

flux, as the front is approached, in a region where the fuel is rapidly depleted, as shown in Fig. 6, mainly by reaction 165f: $NH_3 + OH \rightarrow NH_2 + H_2O$.

(iv) The diffusion of amino radical $D(NH_2)$ promotes the impact of the mode far from the flame front ($P^e_{di,NH_2} > 0$) and opposes it when close to it ($P^e_{di,NH_2} < 0$). This behaviour is due to the location of the peak of NH_2, shown in Fig. 6. Before the peak, diffusion accumulates these species upstream, thus supporting the chemical activity there of the promoting reactions 154f: $NH_2 + NO \rightarrow NNH + OH$ and 163b: $NH_3 + H \leftarrow NH_2 + H_2$, which dominate the combined action of the opposing reactions 153f: $NH_2 + NO \rightarrow N_2 + H_2O$ and 161f: $NH_2 + H\ (+\ M) \rightarrow N_3\ (+\ M)$; $P^e_{154f} + P^e_{163b} > |P^e_{153f} + P^e_{161f}|$. After the peak, diffusion removes NH_2 from a region close to the flame front, where the combined action of the opposing reactions 153f and 161f weaken significantly the dominance of the promoting action of 154f and 163b.

(v) In the 0%-H_2 case, the diffusion of hydrogen $D(H_2)$ promotes the impact of the mode far from the front ($P^e_{di,H_2} > 0$) and opposes it when close to it ($P^e_{di,H_2} < 0$). This behaviour is due to the location where the diffusion of H_2 changes sign, at a point before the peak of the profile of H_2 shown in Fig. 6. Before that point, diffusion accumulates these species upstream, thus supporting the action of reactions 13f: $H_2 + OH \rightarrow H_2O + H$ and

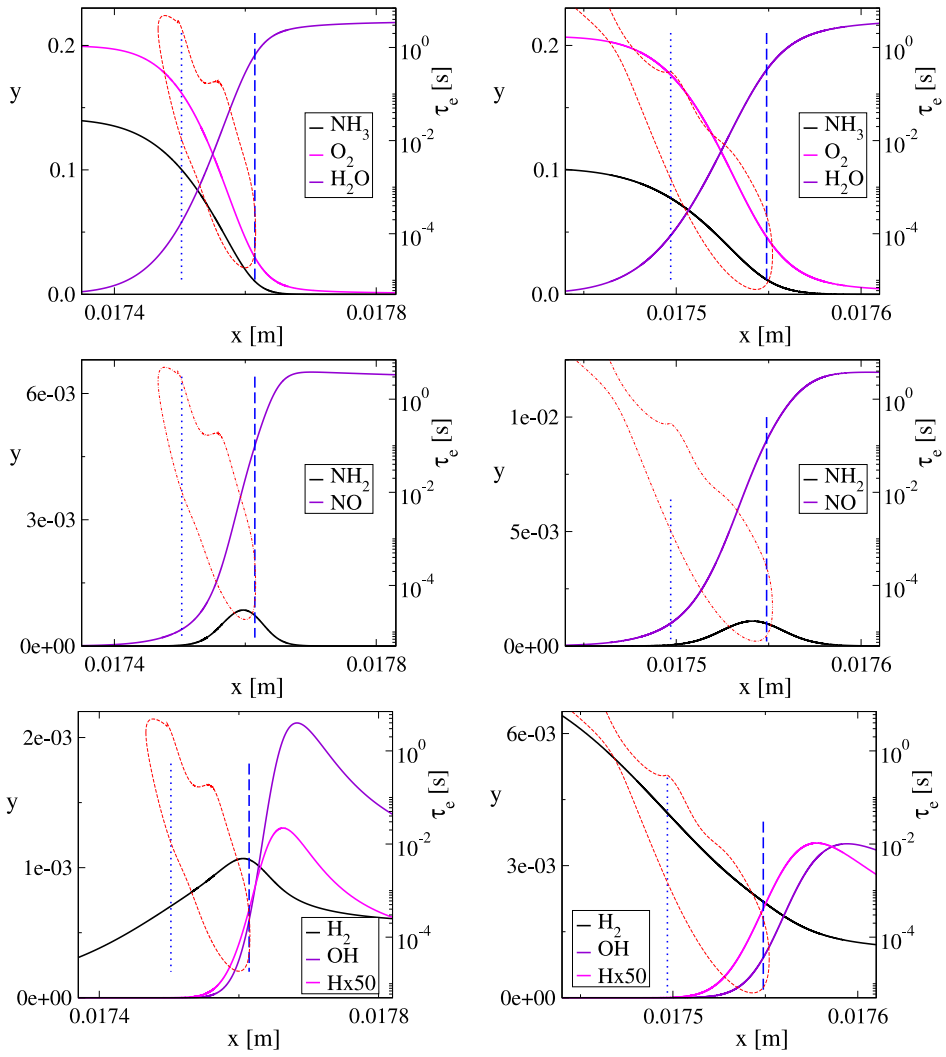

Fig. 6. Mass fraction profiles of various species and the explosive time scale for the 0%-H_2 case (left) and 40%-H_2 case (right); T_o = 600 K, p_o = 10 bar, ϕ = 1. The vertical dotted and dashed lines as in Fig. 4.

163b: $NH_3 + H \leftarrow NH_2 + H_2$. After this point, diffusion removes H_2 from a region close to the flame front towards downstream, weakening the influence of these two reactions. In the 40%-H_2 case, the diffusion hydrogen $D(H_2)$ far from the flame front opposes the impact of the explosive mode there, while has a minor influence close to the front. In this case, the profile of H_2 shown in Fig. 6 indicates that ahead of the flame front diffusion removes this species towards downstream, thus weakening the promoting H-producing reactions 13f, 163b and 11f: $O + H_2 \rightarrow H + OH$. Close to the front, Fig. 6 indicates that a large amount of H has been generated and exhibits a significant influence on the impact of the mode via its diffusion $D(H)$, as shown in Fig. 5. As a result, H_2-diffusion has only minor influence there.

(vi) The diffusion of oxygen $D(O_2)$ opposes the impact of the mode after the P^e_{che} = 0.01 mark ($P^e_{di,O_2} < 0$) and promotes it at the end of the explosive region ($P^e_{di,O_2} > 0$). The diffusion of O_2 follows exactly the same trend as NH_3, i.e., the fuel. The only difference is that at the end $D(O_2)$ becomes positive. In fact, in that region both $D(O_2)$ and $C(O_2)$ become positive. In that region the dominant reaction by far is 12f which consumes O_2. Reaction 9f (also consuming O_2) has a secondary role.

The chemical activity within the explosive mode around the P^e_{che} = 0.01 mark is manifested in both 0% and 40%-H_2 cases first by the NH_2-consuming reactions 154f: $NH_2 + NO \rightarrow NNH + OH$ that promotes the impact of the explosive mode ($P^e_{ce,k} > 0$) and 153f: $NH_2 + NO \rightarrow N_2 + H_2O$ that opposes it ($P^e_{ce,k} < 0$). These are the reactions exhibiting the largest API in the neighbourhood of the $P^e_{che} = 0.01$ mark. The third and fourth panels of Fig. 5 show that beyond this point the promoting reaction 154f is joined by reaction 12f: $H + O_2 \rightarrow OH + O$, followed in a distance by 13f: $H_2 + OH \rightarrow H_2O + H$, 223b: $H + NO (+ M) \leftarrow HNO (+ M)$, 163b: $NH_3 + H \leftarrow NH_2 + H_2$ and in the 40%-H_2 case by reaction 11f: $H_2 + O \rightarrow H + OH$. It is also shown that, in addition to reaction 153f, reactions opposing the impact of the mode are 161f: $NH_2 + H (+ M) \rightarrow NH_3 (+ M)$, 163f: $NH_3 + H \rightarrow NH_2 + H_2$, 9f: $H + O_2 (+ M) \rightarrow HO_2 (+ M)$, 165f: $NH_3 + OH \rightarrow NH_2 + H_2O$, 153f: $NH_2 + NO \rightarrow N_2 + H_2O$ and 13b: $H_2 + OH \leftarrow H_2O + H$. Of all these reactions, the OH-producing reaction 12f is the dominant one, as clearly shown in Fig. 5. As with the reactions contributing the most to the explosive character of τ_e, the findings reported in Fig. 5 indicate the reactions promoting the impact of this mode lead to the production of mainly OH and secondary of H, while the opposing reactions are those that deplete reactants of the promoting ones; such as NH_2, NO and H.

3.2.3. The role of convection of H_2

Having identify the diffusive, convective and chemical processes that contribute the most to the impact of the explosive mode in both 0%-H_2 and 40%-H_2 cases, the effect of the presence of H_2 in the initial mixture can be assessed by examining the influence of the net

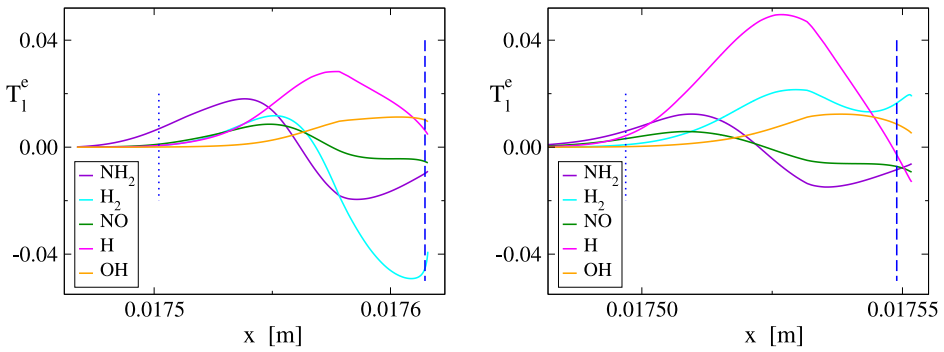

Fig. 7. Profiles of net transport APIs of the explosive mode, $T_l^e = P_{co,l}^e + P_{di,l}^e$ for the 0%-H_2 case (left) and 40%-H_2 case (right); T_o = 600 K, p_o = 10 bar, $\phi = 1$. The vertical dotted and dashed lines as in Fig. 4.

contribution of transport. For that purpose, the index T_l^e $(l = 1, N+1)$ is introduced as:

$$T_l^e = P_{co,l}^e + P_{di,l}^e \tag{4}$$

which accounts for both the convective and diffusive APIs. A comparison of the T_l^e profiles displayed in Fig. 7 with the $P_{di,l}^e$ profiles shown in the second raw of Fig. 5, both related to the species exhibiting a significant contribution to the impact of the explosive mode via their diffusive transport, reveal the following. For the 0%-H_2 case the T_l^e and $P_{di,l}^e$ profiles are qualitatively similar, indicating that the convection of these species has no significant influence in the explosive mode. However, for the 40%-H_2 case a significant difference is revealed, regarding the profiles related to H_2, which is now present in the initial mixture. In particular, while the diffusion of H_2 far from the flame opposes the impact of the mode and close to the flame has a minor promoting influence, the net transport of H_2 is shown to consistently promote the impact of the explosive mode. Apparently, this is a manifestation of a strong promoting influence of the convection of H_2. This influence is due to the increasing consumption of this species in the 40%-H_2 case, relative to the 0%-H_2 case, via reactions 13f: $H_2 + OH \rightarrow H_2O + H$, 163b: $NH_3 + H \leftarrow NH_2 + H_2$ and 11f: $O + H_2 \rightarrow H + OH$, as stated earlier.

3.3. Flame front propagation mechanism

Given that in both 0% and 40%-H_2 cases reactions 154f: $NH_2 + NO \rightarrow NNH + OH$ and 12f: $H + O_2 \rightarrow OH + O$ exhibit the largest contributions in promoting the character and impact of the explosive mode (the former far from the flame front and the latter closer to it), and they produce the radical OH, which is the reactant of the most exothermic reactions 13f: $H_2 + OH \rightarrow H_2O + H$ and 165f: $NH_3 + OH \rightarrow NH_2 + H_2O$, it is concluded that these are the reactions that drive the mechanism for the flame front propagation. The heat released, which was shown to reach a maximum in the rear part of the explosive region and the chemical activity generated there, produce an upstream transport via diffusion of heat, NH_2, NO, H and H_2, which initiate chemical activity ahead of the flame front. The presence of H_2 in the initial mixture reinforces the influence of mainly the driving hydrogen reactions 12f and 13f and secondary of the nitrogen reaction 163b: $NH_3 + H \leftarrow NH_2 + H_2$, leading to a faster flame propagation.

3.4. The case of lean mixtures

The analysis is now extended to fuel lean conditions, due to their relevance to applications such as spark ignition engines and gas turbines [20,45–47]. The findings will be compared with those of the $\phi = 1.0$ case discussed previously.

Fig. 8 displays profiles of the explosive time scales in the spatial domain where they attain minimum values and the temperature undergoes the steep rise, as they were computed for $\phi = 1.0$, 0.8 and 0.6. In order to accommodate all three profiles in a single plot, the linear translation $x \rightarrow x^* = x - x_m$ of the x-axis is employed, where x_m is the location of the maximum dT/dx. It is shown in Fig. 8 that the profiles of τ_e are qualitatively similar. Minor differences are displayed between the $\phi = 0.8$ and 0.6 cases and even smaller between the $\phi = 1.0$ and 0.8 cases. Since the $\phi = 0.8$ case is not that much different from the $\phi = 1.0$ one, in the following only the $\phi = 0.6$ case will be considered.

As in the $\phi = 1.0$ case, the profiles of P_{dif}^e, P_{con}^e and P_{che}^e in the $\phi = 0.6$ case, displayed in Fig. 9, indicate that chemical activity within the explosive mode is first recorded at about the $P_{che}^e = 0.01$ mark for both the 0%-H_2 and 40%-H_2 mixtures; upstream from this point convection balances diffusion. CSP diagnostics show that downstream the $P_{che}^e = 0.01$ mark the explosive dynamics are still dominated by reaction 12f: $H + O_2 \rightarrow OH + O$, as in the $\phi = 1.0$ case discussed previously. Therefore, the interesting question is whether variations in ϕ can cause changes in the initiation of chemical activity. This issue will be examined next, by studying the CSP diagnostics at the indicative point where $P_{che}^e = 0.01$, at which T = 1326.5 K for the 0%-H_2 mixture and T = 1088.7 K for the 40%-H_2 mixture.

Displayed in Table 1 are the reactions that exhibit the largest time scale participation indices for the explosive mode J_k^e at the point where $P_{che}^e = 0.01$ for the 0%-H_2 and 40%-H_2 mixtures and for $\phi = 0.6$. It is shown that in both cases reactions 12f: $H + O_2 \rightarrow OH + O$ and 154f: $NH_2 + NO \rightarrow NNH + OH$ are the ones promoting the most the explosive character of the mode, as at the same stage in the $\phi = 1.0$ case; see Fig. 4. Moreover, the influence of reaction 12f increases and that of 154f decreases in the 40%-H_2 mixture, when compared to their influence in the 0%-H_2 mixture, similarly to the $\phi = 1.0$ case. In addition, Table 1 shows that the promoting influence of reaction 165f: $NH_3 + OH \rightarrow NH_2 + H_2O$ in the 0%-H_2 mixture evolves in an opposing one in the 40%-H_2 mixture, as in the $\phi = 1.0$ case. Another similarity is exhibited by the promoting influence of reaction 13f: $H_2 + OH \rightarrow H_2O + H$, which is shown stronger in the 40%-H_2 mixture. Considering the reactions that promote the explosive character of the mode, the major difference between the $\phi = 1.0$ and $\phi = 0.6$ cases is recorded in the 40%-H_2 mixture. Specifically, the prominent (due to the H_2 addition) role of the OH-producing reaction 11f: $H_2 + O \rightarrow H + OH$ in the $\phi = 1.0$ case is now assigned to the OH-producing reaction 10f: $H_2O_2(^+M) \rightarrow OH + OH(^+M)$. Regarding the reactions opposing the explosive character of the mode, it is shown in Table 1 that these are similar to those in the $\phi = 1.0$ case; i.e., reactions 232f, 153f, 163f, 9f, 153f and 165f (only in the 40%-H_2 mixture) that deplete reactants (NH_2, NO, OH, H, etc.) of the major promoting reactions. In summary, a comparison of the reactions that promote or oppose the explosive character of the mode in the $\phi = 1.0$ and 0.6 cases did not revealed a significant qualitative difference at the spatial point where chemical activity initiates.

In order to examine the chemistry-transport interactions that are recorded within the explosive mode in the $\phi = 0.6$ case at the $P_{che}^e = 0.01$ mark, the largest *API* indices P_x^e are listed in Table 2 for both the 0%-H_2 and 40%-H_2 mixtures. For the 0%-H_2 mixture, the displayed

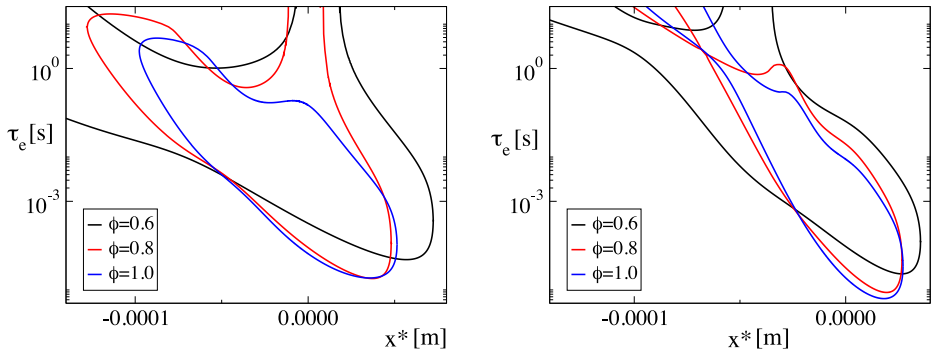

Fig. 8. Profiles of the explosive time scale τ_e in the 0%-H_2 (left) and 40%-H_2 (right) mixtures for $\phi = 1.0$, 0.8 and 0.6; T_o = 600 K, p_o = 10 bar. x^* is the new spacial coordinate, defined as $x^* = x - x_m$, where x_m denotes the point at which the temperature gradient reaches maximum value.

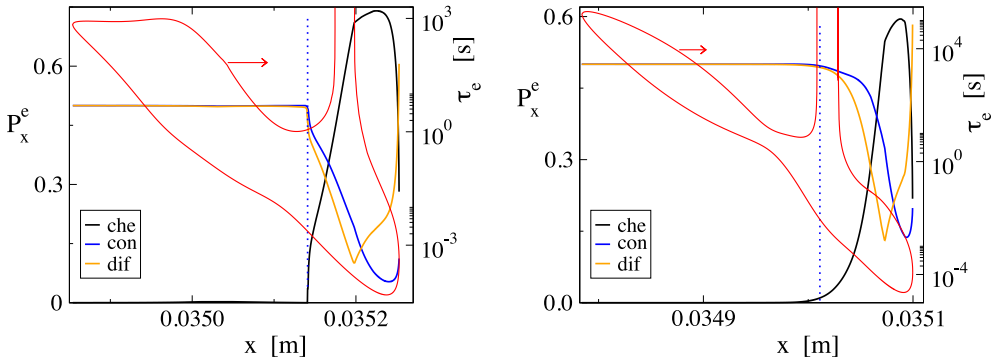

Fig. 9. Profiles of P^e_{dif}, P^e_{con}, P^e_{che} and the explosive time scale τ_e for the 0%-H_2(left) and 40%-H_2 (right) mixtures; T_o = 600 K, p_o = 10 bar, $\phi = 0.6$. The vertical dotted line denotes the point where $P^e_{che} = 0.01$.

Table 1
The major time scale participation indices for the explosive mode J^e_k at the point where $P^e_{che} = 0.01$ for the 0%-H_2 and 40%-H_2 mixtures; T_o = 600 K, p_o = 10 bar, $\phi = 0.6$.

0%-H_2 mixture			
Promoting		Opposing	
12f: $H + O_2 \rightarrow OH + O$	13.02	153f: $NH_2 + NO \rightarrow N_2 + H_2O$	-7.02
154f: $NH_2 + NO \rightarrow NNH + OH$	11.65	232f: $HNO + NH_2 \rightarrow NH_3 + NO$	-5.60
165f: $NH_3 + OH \rightarrow NH_2 + H_2O$	3.38	9f: $H + O_2(+M) \rightarrow HO_2(+M)$	-2.55
151f: $NH_2 + O_2 \rightarrow H_2NO + O$	2.97	219f: $N_2H_4 + OH \rightarrow NH_3 + H_2NO$	-1.91
145f: $NH_2 + O \rightarrow HNO + H$	1.61	245f: $H_2NO + NH_2 \rightarrow HNO + NH_3$	-1.87
13f: $H_2 + OH \rightarrow H_2O + H$	1.25	163f: $NH_3 + H \rightarrow NH_2 + H_2$	-1.30
40%-H_2 mixture			
Promoting		Opposing	
12f: $H + O_2 \rightarrow OH + O$	15.68	165f: $NH_3 + OH \rightarrow NH_2 + H_2O$	-4.16
154f: $NH_2 + NO \rightarrow NNH + OH$	8.76	232f: $HNO + NH_2 \rightarrow NH_3 + NO$	-3.96
13f: $H_2 + OH \rightarrow H_2O + H$	5.06	153f: $NH_2 + NO \rightarrow N_2 + H_2O$	-3.94
10f: $H_2O_2(+M) \rightarrow OH + OH(+M)$	3.02	9f: $H + O_2(+M) \rightarrow HO_2(+M)$	-2.10
244f: $H_2NO + HO_2 \rightarrow HNO + H_2O_2$	2.93	245f: $H_2NO + NH_2 \rightarrow HNO + NH_3$	-2.04
291f: $HONO + NH_2 \rightarrow NO_2 + NH_3$	2.18	213f: $NH_2 + NH_2(+M) \rightarrow N_2H_4(+M)$	-1.96

results lead to the same conclusions that were drawn in the $\phi = 1.0$ case. In particular, it is shown that the largest contribution is provided by the diffusion and convection of heat; the former promoting the impact of the mode and the latter opposing it, exactly as in the $\phi = 1.0$ case. In addition, the species H_2, H_2O, NH_3, O_2 keep behaving as energy buffers. This is manifested by the promoting influence of the diffusion of NH_3 and O_2 towards the flame and the opposing influence of the diffusion of H_2 and H_2O towards the cold reactants. Relative to the $\phi = 1.0$ case, the transport of N_2 is shown to exhibit a larger contribution, as expected for a lean mixture. Its influence is that of an energy buffer, since its upstream diffusion is shown to have an opposing influence; see Fig. 10 for mass fraction profiles of N_2, showing that at the $P^e_{che} = 0.01$ mark the profile has a positive slope. Similarly to the $\phi = 1.0$ case, the upstream diffusion of NO, NH_2 and H is shown to have a promoting influence along with reactions 154f: $NH_2 + NO \rightarrow NNH + OH$, 163b: $NH_3 + H \leftarrow NH_2 + H_2$ and 12f: $H + O_2 \rightarrow OH + O$, while reaction 153f: $NH_2 + NO \rightarrow N_2 + H_2O$ is shown to exhibit the major opposing influence, as in the $\phi = 1.0$ case. All these findings lead to the conclusion that for the 0%-H_2 mixture there is no significant qualitative difference in the transport-chemistry interactions (thus of the flame propagation mechanism) between the $\phi = 1.0$ and 0.6 cases.

The picture that emerges from the *APIs* in the $\phi = 0.6$ case of the 40%-H_2 mixture at the $P^e_{che} = 0.01$ mark exhibits some noticeable differences. It is shown in Table 2 that transport of heat does not provide the largest contribution, although diffusion and convection keep promoting and opposing, respectively, the impact of the mode, as in the $\phi = 1.0$ case. The largest contributions are now provided by the transport of species that were previously acting as energy buffers; e.g., NH_3, H_2O

and O_2. A similar trend is exhibited by N_2 and N_2O, which now contribute much more than in the 0%-H_2 mixture. The only exception is the influence of the transport of H_2, which now reduces considerably. The additional interesting feature is that the influence of the transport of these species is now reversed; the diffusion towards the flame of the species whose mass fraction decreases with distance (NH_3, O_2 and H_2) has an opposing influence, while the diffusion away from the flame towards the cold reactants of the species whose mass fraction increases with distance (N_2 and H_2O) has a promoting influence. Regarding the key species NH_2 and NO that are both reactants of the major promoting reaction 154f, Table 2 shows that their upstream transfer by diffusion has a promoting effect, exactly as in the 0%-H_2 mixture. Despite these significant changes in the manner by which transport contributes to the impact of the explosive mode, the contributions from chemistry are quite similar to the 0%-H_2 mixture. It is shown in Table 2 that for the 40%-H_2 mixture reaction 154f: $NH_2 + NO \rightarrow NNH + OH$ provides the largest contribution, assisted by the H-producing reaction 223b: $H+NO(^+M) \leftarrow HNO(^+M)$ and reaction 12f: $H+O_2 \rightarrow OH+O$. Reactions 154f and 12f were shown to provide the largest and third largest, respectively, contributions in the $\phi = 1.0$ case, while the H-producing reaction 163b: $NH_3+H \leftarrow NH_2+H_2$ was contributing the second largest contribution, instead of reaction 223b in the 0%-H_2 mixture. Similarly, Table 2 shows that the largest opposing contribution is exhibited by reaction 153f: $NH_2+NO \rightarrow N_2+H_2O$, exactly as in the 0%-$H_2$ mixture.

Apparently, the main difference in the cases of 0%-H_2 and 40%-H_2 mixtures is the influence of diffusion. In particular, diffusion of heat exhibits a qualitatively similar influence, but much more diminished in the case of the 40%-H_2 mixture. In addition, the influence of downstream diffusion of species in the cold mixture and that of hot species that diffuse upstream becomes stronger and gets reversed in the 40%-H_2 mixture; i.e., from promoting in the 0%-H_2 mixture to opposing in the 40%-H_2 mixture. Finally, the influence of diffusion of H_2 diminishes significantly in the 40%-H_2 mixture. Regarding the influence of chemistry, the most profound change is in the top 3 promoting reactions; i.e., the prevailing in the 0%-H_2 mixture reaction 163b: $NH_3+H \leftarrow NH_2+H_2$ is replaced in the 40%-H_2 mixture by 223b: $H + NO(^+M) \leftarrow HNO(^+M)$.

All these differences can be explained on the basis of the lower temperature that characterises the case of the 40%-H_2 mixture in the neighbourhood of the $P^e_{che} = 0.01$ mark. In particular, the decreased contribution of heat diffusion relative to the 0%-H_2 mixture is directly related to the increased ones of the species' diffusion. This is manifested by the reversal of the influence of diffusion of all species. While in the 0%-H_2 mixture these species were simply absorbing the incoming heat via the strong action of diffusion, in the 40%-H_2 mixture, where the action of diffusion is weak, these species are acting as energy carriers; either from the hot flame domain to the $P^e_{che} = 0.01$ mark, if they diffuse upstream (thus promoting the action of the mode, as H_2O, N_2 and N_2O) or away from the $P^e_{che} = 0.01$ mark, if they diffuse downstream (thus opposing the action of the mode, as NH_3 and O_2). The lower temperature is to a large extend also responsible for the fact that reaction 163b: $NH_3 + H \leftarrow NH_2 + H_2$ prevails in the 0%-H_2 mixture and reaction 223b: $H + NO(^+M) \leftarrow HNO(^+M)$ prevails in the 40%-H_2 mixture. The differences in the temperature at the $P^e_{che} = 0.01$ mark ($T = 1326.5$ K for the 0%-H_2 mixture and $T = 1088.7$ K for the 40%-H_2 mixture) favour the high activation energy reaction 163b in the 0%-H_2 mixture and the negative activation energy reaction 223b in the 40%-H_2 mixture.

3.5. Validation of CSP diagnostics

It was shown in Fig. 4 that NO tends to promote the explosive character of the mode via 154f: $NH_2+NO \rightarrow NNH+OH$ and to oppose it via 153f: $NH_2 + NO \rightarrow N_2 + H_2O$, the influence of the former being much stronger. Indeed, as shown in Table 3, adding NO in the initial mixture tends to increase the LBV for both 0% and 40%-H_2 mixtures, in agreement to the CSP diagnostics.

It was further shown that reactions 11f: $H_2 + O \rightarrow H + OH$, 12f: $O_2 + H \rightarrow OH + O$ and 13f: $H_2 + OH \rightarrow H_2O + H$ promote the character of the explosive mode, by contributing to a faster τ_e; see the results displayed in Fig. 4. For both mixtures considered, it was shown in Fig. 4 that reaction 12f exhibited the largest influence, followed by reaction 13f and then by 11f. In addition, it was shown that the promoting influence of all reactions was greater in the 40%-H_2 case; reaction 11f exhibiting the most pronounced difference, followed by reaction 13f. The conclusions drawn from the TPIs displayed in Fig. 4 are validated here by comparing the flame speed S_L computed on the basis of the nominal values of the kinetics parameters with the flame speed $S_{L,r}$ obtained by increasing the pre-exponential Arrhenius constant of each of these three reactions by 50%; while keeping that of their backward steps constant. The results shown on Table 4 indicate that the perturbation imposed resulted in a larger flame speed for all cases considered, in agreement to the influence of these reactions in promoting the explosive character of the mode. In addition, the results on Table 4 verify the strongest influence of reaction 12 and the weakest of reaction 11f. Moreover, these results demonstrate the strongest influence of these reactions in the 40%-H_2 case, the difference being more pronounced in the case of reaction 11f, followed by reaction 13f, in agreement to the CSP diagnostics.

Table 2
The major amplitude participation indices for the explosive mode $P^e_{co,n}$, $P^e_{di,n}$ and $P^e_{ch,k}$ at the point where $P^e_{che} = 0.01$; $T_o = 600$ K, $p_o = 10$ bar, $\phi = 0.6$. For convenience, $P^e_{co,n}$ is denoted by $C(y_n)$, $P^e_{di,n}$ is denoted by $D(y_n)$ and $P^e_{ck,k}$ is denoted by $R(k)$.

0%-H_2				40%-H_2			
Promoting		Opposing		Promoting		Opposing	
D(T)	35.04	C(T)	−37.41	C(NH_3)	14.09	C(H_2O)	−16.11
C(H_2)	3.62	D(H_2)	−3.34	D(H_2O)	13.66	D(NH_3)	−12.27
C(H_2O)	3.14	D(H_2O)	−3.01	C(O_2)	6.91	C(T)	−7.91
D(NH_3)	2.74	C(NH_3)	−2.53	D(T)	6.45	D(O_2)	−6.18
D(NO)	1.29	C(NO)	−0.72	D(N_2)	3.56	C(N_2)	−4.36
D(NH_2)	1.15	D(N_2)	−0.40	D(NO)	1.18	C(N_2O)	−0.69
R(154f)	0.49	C(O_2)	−0.40	D(NH_2)	0.96	R(153f)	−0.58
C(N_2)	0.44	R(153f)	−0.38	D(N_2O)	0.66	C(NO)	−0.32
D(O_2)	0.38	C(NH_2)	−0.23	R(154f)	0.61	C(NH_2)	−0.22
D(H)	0.29			R(12f)	0.28		
R(163b)	0.26			D(H_2)	0.23		
R(12f)	0.25			R(223b)	0.17		

Table 3
S_L with NO addition (molar) to the initial mixture; $T_o = 600$ K, $p_o = 10$ bar, $\phi = 1$.

NH_3/NO	S_L [m/s]	$NH_3/H_2/NO$	S_L [m/s]
100% / 0%	0.188	60.0% / 40.0%/ 0%	0.4844
97% / 3%	0.210	58.2% / 38.8%/ 3%	0.5457
94% / 6%	0.237	56.4% / 37.6%/ 6%	0.6154

Table 4
The flame sped S_L [m/s] and the percentage change in $\Delta S_L = (S_{L,r} - S_L)/S_L$ when the pre-exponential Arrhenius constant of reactions r =11f, 12f and 13f is perturbed by 50%; $T_o = 600$ K, $p_o = 10$ bar, $\phi = 1.0, 0.8, 0.6$.

%-H_2	ϕ	S_L [m/s]	$\Delta S_{L,11f}$	$\Delta S_{L,12f}$	$\Delta S_{L,13f}$
0	1.0	0.188	0.85	30.99	5.59
0	0.8	0.145	0.69	28.77	5.78
0	0.6	0.071	0.28	29.31	5.07
40	1.0	0.483	3.26	33.67	9.04
40	0.8	0.356	2.72	30.70	9.18
40	0.6	0.193	1.92	31.97	9.48

4. Conclusions

In the region of the flame where the explosive mode encapsulates non-negligible chemical activity, significant conclusions regarding the

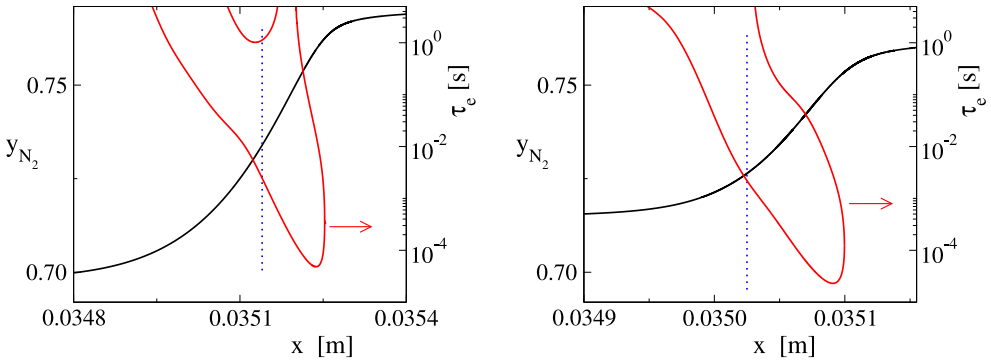

Fig. 10. Profiles of the mass fraction of N_2 and the explosive time scale τ_e for the 0%-H_2(left) and 40%-H_2 (right) mixtures; T_o = 600 K, p_o = 10 bar, $\phi = 0.6$. The vertical dotted line denotes the point where $P^e_{che} = 0.01$.

mechanism of its front propagation can be reached. Considering NH_3 and NH_3/H_2 stoichiometric mixtures with air under engine-relevant conditions, it was shown that this mechanism shares some similarities with that of hydrocarbons; such as the upstream diffusion of heat and H radicals that originate from the high-temperature region. However, the picture emerging with ammonia is much more complex regarding the species that diffuse and the dominant reactions; such as the upstream diffusion of NH_2 and NO and the crucial role ahead of the flame front of the negative-activation-energy reaction 154f: $NH_2 + NO \rightarrow NNH + OH$. Most likely, this is due to the differences in the prevailing oxidation paths; via alkoxy radicals R-O-O- to CO_2 for hydrocarbons and via a more complex path to N_2 for ammonia [48].

The presence of hydrogen in the initial mixture, even in a small amount, was shown to increase LBV by reinforcing the underlying propagation mechanism rather than introducing a different mechanism. This influence of hydrogen is manifested by its enhanced downstream convective transport that is caused by its increased consumption by reactions that provide significant contributions to the explosive dynamics. Additionally, it is demonstrated that an explosive mode can provide meaningful results only when there is significant chemical activity recorded within the amplitude of the mode. This issue is overlooked by the Chemical Explosive Mode Analysis method, which assumes that τ_e is always the characteristic one [49,50], and as such it can lead to wrong conclusions [51,52].

A preliminary investigation indicated that the flame front propagation mechanism in the case of lean mixtures is similar to that of stoichiometric mixtures, only when pure ammonia fuel is considered. The presence of H_2 in the initial lean mixture diminished the influence of the upstream diffusion of heat and caused the reversal of the influence of some species' transport, leaving the dominant chemistry intact. These changes were attributed to the prevailing lower temperatures ahead of the flame and the decreased role of the upstream diffusion of heat. The issue of the lean mixtures deserves a more thorough investigation.

Addressing these complexities and acknowledging the role of transport and diverse chemical pathways not only enriches our fundamental understanding of NH_3 and H_2-enriched flame propagation but also offers essential insights for leveraging ammonia's potential in driving forward sustainable energy transition strategies. By probing the fundamental mechanism of propagation with CSP-powered asymptotic analysis, the proposed methodology herein holds promise for enhancing our understanding and control of flames across a wider range of fuels.

CRediT authorship contribution statement

Efstathios-Al. Tingas: Writing – original draft, Visualization, Software, Investigation, Formal analysis. **Savvas Gkantonas:** Writing – original draft, Visualization, Software, Investigation, Formal analysis. **Epaminondas Mastorakos:** Writing – review & editing, Investigation, Funding acquisition, Conceptualization. **Dimitris Goussis:** Writing – review & editing, Investigation, Funding acquisition, Conceptualization.

Declaration of competing interest

The authors declare that they have no known competing financial interests or personal relationships that could have appeared to influence the work reported in this paper.

Acknowledgements

SG and EM acknowledge funding from the European Union's Horizon 2020 CoEC project, grant agreement No 952181. DAG acknowledges partial support from Khalifa University of Science and Technology, United Arab Emirates, via project RC2-2019-007.

Appendix A. Supplementary data

Supplementary material related to this article can be found online at https://doi.org/10.1016/j.ijhydene.2024.06.289.

References

[1] Kobayashi H, Hayakawa A, Somarathne KKA, Okafor EC. Science and technology of ammonia combustion. Proc Combust Inst 2019;37(1):109–33.
[2] Valera-Medina A, Amer-Hatem F, Azad AK, Dedoussi IC, de Joannon M, Fernandes RX, et al. Review on ammonia as a potential fuel: From synthesis to economics. Energy Fuels 2021;35(9):6964–7029
[3] Ichikawa Y, Niki Y, Takasaki K, Kobayashi H, Miyanagi A. NH3 combustion using three-layer stratified fuel injection for a large two-stroke marine engine: Experimental verification of the concept. Appl Energy Combust Sci 2022;10:100071.
[4] Mounaïm-Rousselle C, Mercier A, Brequigny P, Dumand C, Bouriot J, Houillé S. Performance of ammonia fuel in a spark assisted compression Ignition engine. Int J Engine Res 2022;23(5):781–92.
[5] Guiberti TF, Pezzella G, Hayakawa A, Sarathy SM. Mini review of ammonia for power and propulsion: Advances and perspectives. Energy Fuels 2023;37(19):14538–55.
[6] Lee J, Kim J, Park J, Kwon O. Studies on properties of laminar premixed hydrogen-added ammonia/air flames for hydrogen production. Int J Hydrog Energy 2010;35(3):1054–64.
[7] Ichikawa A, Hayakawa A, Kitagawa Y, Somarathne KKA, Kudo T, Kobayashi H. Laminar burning velocity and markstein length of ammonia/hydrogen/air premixed flames at elevated pressures. Int J Hydrog Energy 2015;40(30):9570–8.
[8] Cheng M, Wang H, Xiao H, Luo K, Fan J. Emission characteristics and heat release rate surrogates for ammonia premixed laminar flames. Int J Hydrog Energy 2021;46(24):13461–70.
[9] Tang G, Jin P, Bao Y, Chai WS, Zhou L. Experimental investigation of premixed combustion limits of hydrogen and methane additives in ammonia. Int J Hydrog Energy 2021;46(39):20765–76.
[10] Osipova KN, Korobeinichev OP, Shmakov AG. Chemical structure and laminar burning velocity of atmospheric pressure premixed ammonia/hydrogen flames. Int J Hydrog Energy 2021;46(80):39942–54.

[11] Yang W, Dinesh KR, Luo K, Thevenin D. Direct numerical simulation of turbulent premixed ammonia and ammonia-hydrogen combustion under engine-relevant conditions. Int J Hydrog Energy 2022;47(20):11083–100.
[12] Hu X, Luo C, Chen X, Liu Q, Su M. Study on flame propagation and inherent instability of hydrogen/ammonia/air mixture. Fuel 2024;357:129848.
[13] Thomas DE, Wadkar C, Goertemiller CF, Northrop WF. Structure and nitric oxide formation in laminar diffusion flames of ammonia–hydrogen and air. Fuel 2024;362:130764.
[14] Zhang F, Zhang G, Wang Z, Wu D, Jangi M, Xu H. Experimental investigation on combustion and emission characteristics of non-premixed ammonia/hydrogen flame. Int J Hydrog Energy 2024;61:25–38.
[15] da Rocha RC, Costa M, Bai X-S. Chemical kinetic modelling of ammonia/hydrogen/air ignition, premixed flame propagation and NO emission. Fuel 2019;246:24–33.
[16] Mashruk S, Zitouni S-E, Brequigny P, Mounaim-Rousselle C, Valera-Medina A. Combustion performances of premixed ammonia/hydrogen/air laminar and swirling flames for a wide range of equivalence ratios. Int J Hydrog Energy 2022;47(97):41170–82.
[17] Liang B, Yang M, Gao W, Jiang Y, Li Y. Study on premixed hydrogen-ammonia-air flame evolution in a horizontal rectangular duct. Fuel 2023;354:129427.
[18] Wu Z, Zhang G, Wang C, Jin S, Ji M, Hu C, et al. Numerical investigation on the flame propagation process of ammonia/hydrogen blends under engine-related conditions. Int J Hydrog Energy 2024;60:1041–53.
[19] Alnasif A, Zitouni S, Mashruk S, Brequigny P, Kovaleva M, Mounaïm-Rousselle C, et al. Experimental and numerical comparison of currently available reaction mechanisms for laminar flame speed in 70/30 (% vol.) NH3/H2 flames. Appl Energy Combust Sci 2023;14:100139.
[20] Zhu Y, Curran HJ, Girhe S, Murakami Y, Pitsch H, Senecal K, et al. The combustion chemistry of ammonia and ammonia/hydrogen mixtures: A comprehensive chemical kinetic modeling study. Combust Flame 2024;260:113239.
[21] Han X, Lavadera ML, Konnov AA. An experimental and kinetic modeling study on the laminar burning velocity of NH3+ N2O+ air flames. Combust Flame 2021;228:13–28.
[22] Lewis B, von Elbe G. On the theory of flame propagation. J Chem Phys 1934;2(8):537–46.
[23] Zeldowitsch JB, Frank-Kamenetzki DA. A theory of thermal propagation of flame. Acta Physicochim URS 1938;IX(2).
[24] Williams FA. Progress in knowledge of flamelet structure and extinction. Prog Energy Combust Sci 2000;26(4–6):657–82.
[25] Buckmaster J, Clavin P, Liñán A, Matalon M, Peters N, Sivashinsky G, et al. Combustion theory and modeling. Proc Combust Inst 2005;30(1):1–19.
[26] Matalon M. Flame dynamics. Proc Combust Inst 2009;32(1):57–82.
[27] De Goey LPH, Van Oijen JA, Kornilov VN, ten Thije Boonkkamp JHM. Propagation, dynamics and control of laminar premixed flames. Proc Combust Inst 2011;33(1):863–86.
[28] Lam SH, Goussis DA. Understanding complex chemical kinetics with computational singular perturbation. Symp (Intl) Combust 1989;22(1):931–41.
[29] Hadjinicolaou M, Goussis DA. Asymptotic solution of stiff PDEs with the CSP method: the reaction diffusion equation. SIAM J Sci Comput 1998;20(3):781–810.
[30] Kaper HG, Kaper TJ, Zagaris A. Geometry of the computational singular perturbation method. Math Model Nat Phenom 2015;10(3):16–30.
[31] Lizarraga I, Wechselberger M. Computational singular perturbation method for nonstandard slow-fast systems. SIAM J Appl Dyn Syst 2020;19(2):994–1028.
[32] Valorani M, Najm HN, Goussis DA. CSP analysis of a transient flame-vortex interaction: time scales and manifolds. Combust Flame 2003;134(1–2):35–53.
[33] Najm HN, Valorani M, Goussis DA, Prager J. Analysis of methane-air edge flame structure. Combust Theor Model 2010;14(2):257–94.
[34] Radaideh MI, Manias DM, Kyritsis DC, Goussis DA. OME2- 4/air mixtures: The structure and propagation mechanism of their laminar premixed flames. Fuel 2024;363:131004.
[35] Prager J, Najm HN, Valorani M, Goussis D. Structure of n-heptane/air triple flames in partially-premixed mixing layers. Combust Flame 2011;158(11):2128–44.
[36] Diamantis DJ, Mastorakos E, Goussis DA. H_2/air autoignition: The nature and interaction of the developing explosive modes. Combust Theor Model 2015;19(3):382–433.
[37] Goussis DA, Najm HN. Model reduction and physical understanding of slowly oscillating processes: the circadian cycle. Multiscale Model Simul 2006;5(4):1297–332.
[38] Maas U, Pope SB. Simplifying chemical kinetics: intrinsic low-dimensional manifolds in composition space. Combust Flame 1992;88(3–4):239–64.
[39] Valorani M, Ciottoli PP, Galassi RM. Tangential stretching rate (TSR) analysis of non premixed reactive flows. Proc Combust Inst 2017;36(1):1357–67.
[40] Tingas E-A, Wang Z, Sarathy SM, Im HG, Goussis DA. Chemical kinetic insights into the ignition dynamics of n-hexane. Combust Flame 2018;188:28–40.
[41] Goussis DA, Valorani M, Creta F, Najm HN. Reactive and reactive-diffusive time scales in stiff reaction-diffusion systems. Progr Comput Fluid Dyn Int J 2005;5(6):316–26.
[42] Kazakov A, Chaos M, Zhao Z, Dryer FL. Computational singular perturbation analysis of two-stage ignition of large hydrocarbons. J Phys Chem A 2006;110(21):7003–9.
[43] Nawaz B, Nasim MN, Das SK, Landis J, SubLaban A, Trelles JP, et al. Combustion characteristics and emissions of nitrogen oxides (NO, NO2, N2O) from spherically expanding laminar flames of ammonia–hydrogen blends. Int J Hydrog Energy 2024;65:164–76.
[44] Tingas EA, Kyritsis DC, Goussis DA. Algorithmic determination of the mechanism through which H_2O-dilution affects autoignition dynamics and NO formation in CH_4/air mixtures. Fuel 2016;183:90–8.
[45] Xin G, Ji C, Wang S, Meng H, Chang K, Yang J. Effect of ammonia addition on combustion and emission characteristics of hydrogen-fueled engine under lean-burn condition. Int J Hydrog Energy 2022;47(16):9762–74.
[46] Jin U, Kim KT. Hybrid rich-and lean-premixed ammonia-hydrogen combustion for mitigation of NOx emissions and thermoacoustic instabilities. Combust Flame 2024;262:113366.
[47] Huo J, Zhao T, Lin H, Li J, Zhang W, Huang Z, et al. Study on lean combustion of ammonia-hydrogen mixtures in a pre-chamber engine. Fuel 2024;361:130773.
[48] Manias DM, Patsatzis DG, Kyritsis DC, Goussis DA. NH_3 vs. CH_4 autoignition: A comparison of chemical dynamics. Combust Theor Model 2021;25(6):1110–31.
[49] Lu TF, Yoo CS, Chen JH, Law CK. Three-dimensional direct numerical simulation of a turbulent lifted hydrogen jet flame in heated coflow: a chemical explosive mode analysis. J Fluid Mech 2010;652:45–64.
[50] Shan R, Yoo CS, Chen JH, Lu T. Computational diagnostics for n-heptane flames with chemical explosive mode analysis. Combust Flame 2012;159(10):3119–27.
[51] Goussis DA, Im HG, Najm HN, Paolucci S, Valorani M. The origin of CEMA and its relation to CSP. Combust Flame 2021;227:396–401.
[52] Goussis DA, Valorani M. The appropriate context for the analysis of the explosive mode in reactive systems. J Energy Eng 2023;149:04023039.